Mine Water and the Environment (2020) 39:308–319
https://doi.org/10.1007/s10230-020-00687-6

TECHNICAL ARTICLE

Water–Sediment Two-Phase Flow Inrush Hazard in Rock Fractures of Overburden Strata During Coal Mining

Dan Ma[1,2,3] · Hongyu Duan[1] · Weitao Liu[3] · Xiaotong Ma[1] · Ming Tao[1]

Received: 25 November 2019 / Accepted: 24 April 2020 / Published online: 6 May 2020

Abstract

To investigate the mechanism of water–sediment inrush during coal mining, the characteristics of water–sediment flow in rock fractures were quantitatively analyzed by computational fluid dynamics (CFD). Based on the two-phase flow theory, a resistance model of water–sediment flow in fractures was established and verified by a laboratory-scale test. The results showed that: (1) With increases sediment particle diameter, volume fraction, and initial water phase velocity, the resistance of sediment particles grows gradually. (2) The drag force of sediment particles is mainly generated from the collision of the water phase and fracture wall. The velocity distribution of sediment particles can be divided into three stages, i.e., continuous increase, rapid decrease, and slow fluctuation. (3) The numerical model was shown to have high predictive accuracy by comparison with the test results. The model's predictive accuracy decreases with increased water phase velocity and decreases of the sediment particle diameter and volume fraction. (4) The smaller the fracture width, the larger the inclination and bending angles, and the greater the resistance of the two-phase flow in the fracture. Collisions between the particles and fracture wall cause velocity attenuation of the sediment particles. We propose water–sediment inrush prevention and control technology based on the numerical analysis results.

Keywords Mining rock fracture · Water–sediment fluid · Flow characteristics · CFD numerical simulation

Introduction

Longwall mining is widely applied in western China (Ju et al. 2018; Zhang et al. 2015b). Thin overburden strata are prone to fracture after longwall mining, which can induce an water–sediment inrush disaster (Fan et al. 2018; Peng et al. 2019), during which sediment particles quickly flood into the mining face along with water, resulting in casualties and equipment damage (Elbaz et al. 2016). Water–sediment inrush events can waste large amounts of water and pollute the groundwater (see supplemental Fig. S-1), aggravating regional water shortages (Huang et al. 2019b; Ma et al. 2019b; Sun et al. 2012). In addition, soil erosion caused by disasters can cause other environmental problems, such as subsidence (Zhang et al. 2015a). Therefore, methods to prevent water–sediment inrush disasters and protect water resources are urgently needed in western China's mining area.

Research has shown that mining under unfavorable geological conditions is one of the main causes of water inrush accidents (Ma et al. 2019a, d; Zhang et al. 2014). Gullies formed by historical water erosion are common in arid and

Electronic supplementary material The online version of this article (https://doi.org/10.1007/s10230-020-00687-6) contains supplementary material, which is available to authorized users.

✉ Dan Ma
dan.ma@cumt.edu.cn

✉ Weitao Liu
skdlwt@126.com

1 School of Resources and Safety Engineering, Central South University, Changsha 410083, Hunan, China

2 State Key Laboratory of Coal Resources and Safe Mining, School of Mines, China University of Mining and Technology, Xuzhou 221116, Jiangsu, China

3 State Key Laboratory of Mining Disaster Prevention and Control Co-Founded by Shandong Province and the Ministry of Science and Technology, Shandong University of Science and Technology, Qingdao 266590, Shandong, China

semi-arid regions of western China. These gullies are generally filled with aeolian sand, forming a deep buried channel (Poesen et al. 2003; Valentin et al. 2005). Longwall mining breaks the strata in the caved zone into irregular shapes of various size, while the strata in the fractured zone are broken into blocks by vertical and/or horizontal fractures due to bed separation (Gu et al. 2019; Huang and Yang 2019; Huang et al. 2019a; Tao et al. 2017). As shown in Fig. 1, when the top plate fracture connects with the bottom of one of these gullies, the groundwater and aeolian sand enters the working surface along the fracture, resulting in a water–sediment inrush disaster (Fan et al. 2018; Yang et al. 2019; Zhang et al. 2015a); the roof fissure acts as a water inrush pathway.

Previous researchers have highlighted the seepage process in fractured geological media (Liu et al. 2020; Yang et al. 2019). Berkowitz (2002) regarded the fracture network as groundwater flow channels. In this research, one of the key difficulties was correlating geometrical and hydraulic properties of a fractured formation, particularly in light of the uncertainty in measurements. After this, a series of studies were conducted to investigate the influence of fracture inclination angles (Liang et al. 2019), connectivity (Brouwers and Dippenaar 2019; Guihéneuf et al. 2014), water pressure (Guihéneuf et al. 2014; Huang et al. 2018; Qian et al. 2019) and mining-induced disturbance (Kristinof et al. 2010; Ma et al. 2019c) on the hydraulic characteristics of fractured geological media.

Although the hydraulic characteristics of the fractured rock mass were comprehensively studied in the above studies, the influences of solid particles inside the fluid were not considered. These solid particles both change the hydraulic properties of fractured media and damage the internal structure of the rock mass (Liu et al. 2017, 2018; Wang and Kong 2018). Ma et al. (2017) explored the migration of fine rock particles by two-phase flow experiments in broken sandstone. Their results showed that the sandstone's hydraulic properties were changed by the particles. Wang et al. (2019) established a particle migration model in fractured sandstone during the groundwater inrush process. A series of indoor experiments were conducted on water–sediment two-phase flow in fractured geological media. Liu and Li (2016) analyzed the influence of particle size on non-Darcian seepage of water and sand in fractured rock. Yang et al. (2019) designed and manufactured a test system to simulate the startup, transfer, and inrush of the mixed water and sediment in an overburden fracture channel.

However, due to the scale gap between laboratory tests and the field, indoor experiments cannot fully simulate the issue of fracture seepage at the engineering scale (Hamm et al. 2007; Huang et al. 2016). At the same time, due to the high risk of water–sediment inrush, it is difficult to conduct in-situ simulation tests at the engineering site. Numerical simulation overcomes the scale limitation of indoor experiments and has the advantages of high efficiency, low cost, and predictable results, thus it has been widely used in the research of seepage process in rock and soil (Li et al. 2019; Liu et al. 2019; Zhang et al. 2008; Zhou et al. 2018). Although numerical simulation has been used to simulate the seepage process in fractured media (Fan and Zheng 2013; Javadi et al. 2010; Kristinof et al. 2010; Li et al. 2012; Ren et al. 2017; Xu et al. 2013), numerical simulation of water–sediment two-phase flow in rock fractures has not been reported. Flow resistance characteristics are more complicated in water–sediment two-phase flow; therefore, accurate simulation of this flow in rock fractures is important for the prevention and control of water and sediment inrush disasters.

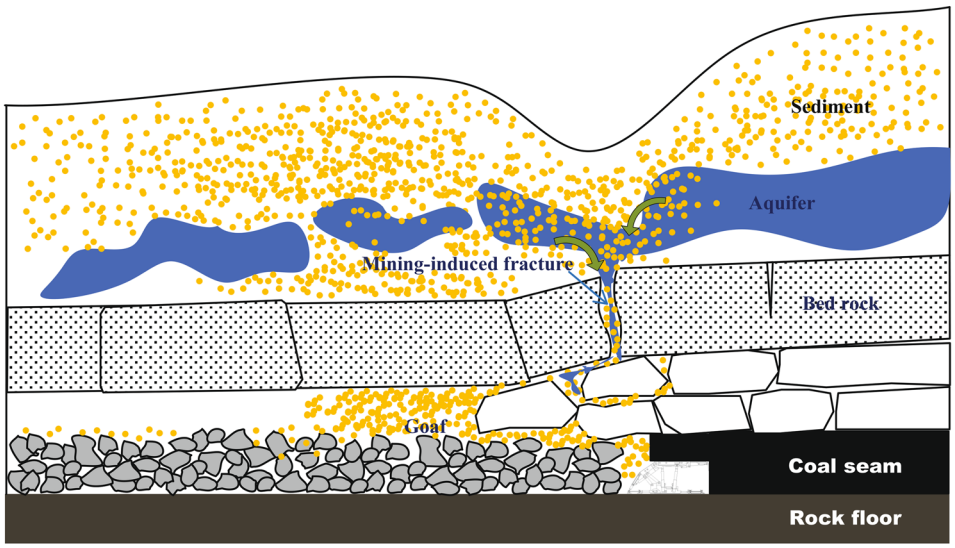

Fig. 1 Schematic diagram of the hydrogeological structure model of water–sediment inrush

In this study, we investigated the potential hazard of mining-induced water–sediment inrush in the Buliangou coal mine. First, based on the geological background, a water–sediment two-phase flow resistance model was established. Then, the influences of fluid and fracture characteristics on water–sediment flow were analyzed. Finally, based on the numerical results, a water–sediment inrush prevention and treatment plan was proposed.

Geological Background

The Buliangou coal mine, located east of Ordos, Inner Mongolia, China (see supplemental Fig. S-2), has typical geomorphic characteristics of the Loess Plateau. The terrain is high in the southwest and low in the northeast, with an elevation of 1127–1346 m. The ground surface is covered by loess and aeolian sand, and bedrock is only exposed in large gullies. Soil erosion in this area is serious, forming a complex terrain with vertical and horizontal gullies and steep deep walls.

Due to the thick coal seam and the thin amount of overlying bedrock at the Buliangou coal mine, the mining-induced water-conducting fracture zone directly reaches the surface, and serious surface subsidence occurs above the goaf (supplemental Fig. S-3). Obvious surface collapses and wide surface fracture occur and in the steep slope area above the goaf, the loess collapses and slips, completely damaging the original loess structure. Since the groundwater level in this area is usually above the elevation of the coal seam roof, groundwater mixed with aeolian sand frequently flows into the rock fracture and underground space during mining. As a result, there is a high risk of water–sediment inrush.

Water–Sediment Two-Phase Flow Resistance Model

Model Hypothesis

For simplicity, water–sediment two-phase flow models require some assumptions (Peker and Helvaci 2008):

1. It was assumed that water acts as a Newtonian fluid and obeys the constitutive relationship of the incompressible viscous flow, and that the sediment phase can be regarded as discrete particles. The pore volume fraction between sediment particles is relatively low and there is no phase transition.
2. Sediment particles are smooth rigid spheres with uniform size, and the probability of collision between the particles is low.
3. Saffman force and other external forces are ignored; only gravity, pressure gradients, buoyancy, resistance, and the Magnus lift of the particles in the flow field are considered.
4. Besides the interaction of the time-averaged motion with the liquid, sediment particles are also subjected to the liquid's turbulent diffusion.
5. Regardless of multi-component and non-isothermal conditions in liquids, the effects of molecular diffusion and Brownian motion on solid-phase particles are ignored.
6. Due to the small length of the fracture channel and the low osmotic pressure, the change in fluid volume along the length of a pore is ignored due to fluid compressibility in the pores.
7. The fracture is assumed to be a circular tube that does not change with the fluid flow; fracture closure is neglected.
8. The permeation of the water phase is not considered.
9. Due to the low volume concentration of the sediment particles, the energy loss caused by the collision of sediment particles is neglected.

Governing Equations

Based on the above assumptions and research by Sahimi (2011), governing equations for the water–sediment two-phase flow model of the fracture include mass and momentum conservation for both the water and sediment phases. The coupling equations of water–sediment phase are summarized as follows:

1. Governing equation of water phase:

$$\begin{cases} \frac{\partial \rho_f}{\partial t} + \nabla \cdot \left(\rho_f v_f\right) = 0 \\ \frac{dv}{dt} = \rho_f g - \frac{1}{\rho_f}\nabla p + \mu \nabla^2 v + \frac{F_{sf}}{\rho_f\left(1-c_s\right)} = 0 \end{cases} \tag{1}$$

where, ρ_f is the density of water phase; v_f is the velocity vector of water phase, c_s is the volume fraction of sediment particles, p is the pore pressure, μ is the dynamic viscosity of the water, and F_{sf} is the force of sediment particles on the water.

2. Governing equation of the sediment phase:

$$\begin{cases} \frac{\partial\left(\rho_s c_s\right)}{\partial t} + \nabla \cdot \left(\rho_s c_s v_s\right) = 0 \\ \left(1 + \frac{1}{2}\frac{\rho_f}{\rho_s}\right)\frac{dv_s}{dt} - \frac{1}{2}\frac{\rho_f}{\rho_s}\frac{dv_f}{dt} + \frac{1}{\rho_s}\frac{\partial p}{\partial x} \\ \quad = \left(\rho_s - \rho_f\right)g + \frac{1}{c_s\rho_s}\left(F_{fs} + F_{ws}\right) \end{cases} \tag{2}$$

where ρ_s is the density of the sediment phase; v_s is the velocity vector of the sediment phase, F_{fs} is the force of the water on sediment particles, and F_{ws} is the equivalent wall resistance in the pores of the dx segment.

3. Water–sediment two-phase coupling equation:

$$F_{fs} = -F_{sf} \tag{3}$$

Auxiliary Equations

Auxiliary equations are presented as follows.

1. Equivalent resistance of pore wall:

$$F_{ws} = \frac{1}{2}\rho_s V_s \left(v_{1,n}^2 - v_{2,n}^2\right) f_{ws} A \tag{4}$$

where f_{ws} is the average collision frequency between sediment particles within the two-phase flow per unit volume and wall surface, which is related to the roughness of the wall surface, and A is the cross-sectional area of the pores.

2. Interactive force of the water–sediment:

$$F_{fs} = \frac{1}{8}\pi d_s^2 \left[C_D \rho_f \left|v_f - v_s\right| \left(v_f - v_s\right) + d_s \rho_s \omega \left(v_f - v_s\right)\right] \tag{5}$$

where ω is the rotation velocity of particles and C_D is the flow parameter and also has:

$$C_D = \begin{cases} \frac{24}{Re_s} & Re_s < 2 \\ \frac{24}{Re_s^{0.6}} & 2 < Re_s < 500 \\ 0.44 & 500 < Re_s < 2 \times 10^5 \end{cases} \tag{6}$$

where Re_s is the Reynolds number of sediment particles.

Numerical Simulation of the Water–Sediment Mixture's Flow Resistance Characteristics

Solution Conditions

The water–sediment two-phase flow resistance model is shown in Fig. 2.

1. Boundary conditions of the water phase

Since the movement of fluid particles in turbulent motion is complicated, the inlet boundary of the water phase is approximated by empirical formulas using previous experimental data, named the "1/7 law":

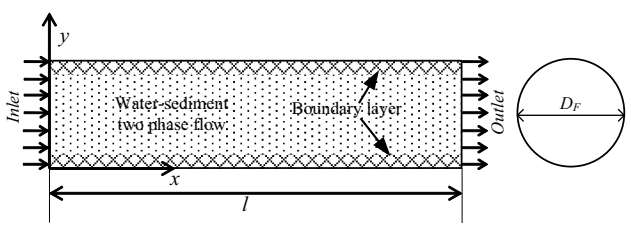

Fig. 2 Resistance model of water–sediment mixed flow

$$v_{f,in} = v_0 \left(1 - d_s / D_F\right)^{\frac{1}{7}} \tag{7}$$

where v_0 is the initial water phase velocity, d_s is the size of particle sediment, D_F is the fracture width.

Assuming that the boundary of the pore surface is non-penetrating and non-slip, then:

$$v_{f,wall} = 0 \tag{8}$$

The outlet boundary is set as:

$$p_{f,outlet} = 0 \tag{9}$$

2. Boundary conditions of the sediment phase

The inlet boundary of the sediment phase is the same as the water phase:

$$v_{s,in} = v_{f,in} = v_0 \left(1 - d_s / D_F\right)^{\frac{1}{7}} \tag{10}$$

Based on the assumption that the impact of rough boundary on sediment particles is equivalent to the boundary layer resistance, so the boundary of the pore surface is considered to be non-penetrating and non-slip:

$$v_{s,wall} = 0 \tag{11}$$

The outlet boundary is set as:

$$p_{s,outlet} = 0 \tag{12}$$

3. Initial conditions

The velocity of the water–sediment two-phase fluid is consistent, and can be expressed as:

$$v_f\big|_{t=0} = v_s\big|_{t=0} = v_0 \left(1 - d_s / D_F\right)^{\frac{1}{7}} \tag{13}$$

At time t = 0, sediment particles are injected from the inlet, and $c_s\big|_{t=0} = 0$ within the fracture.

Numerical Model Scheme

Based on the above assumptions, the fracture channel is regarded as a round, elongated pipe. Computational fluid dynamics software was used to study the influence of factors such as sediment particle diameter, volume fraction, initial water phase velocity, fracture width, inclination angle, and bending angle on the resistance characteristics of the water–sediment two-phase flow. The various parameters and properties of the numerical model were set as: the water phase in the fluid zone is a continuous fluid, with a density of 10^3 kg/m^3; the solid phase is regarded as suspended aeolian sediment particles, with a density of 1420 kg/m^3; the water–sediment fluid enters in a direction perpendicular to the entrance of the fracture. The initial conditions and boundary conditions were stated above, and the pressure at

the outlet boundary is 0 Pa. A non-slip boundary condition was adopted for the wall surface and the standard wall function was used for conditions near the wall.

Numerical Results

Influence of Fluid Characteristics on the Water–Sediment Flow

To investigate the influence of fluid characteristics on the water–sediment flow, sediment particle diameter, volume fraction, and initial water phase velocity were considered. The simulation scheme is shown in Table 1.

Table 1 Numerical schemes of fluid characteristics of water–sediment flow for a fracture width of 10 mm, a fracture inclination and bending angles of 0°

Schemes	Sediment particle diameter (mm)	Sediment particle concentration (%)	Initial water phase velocity (m s^{-1})
Scheme 1 Sediment particle diameter	0.08, 0.12, 0.16, 0.20	4	0.2
Scheme 2 Sediment particle concentration	0.12	2, 4, 6, 8	0.2
Scheme 3 Initial water phase velocity	0.12	4	0.1, 0.2, 0.3

Sediment Particle Diameter

Figure 3 shows the trajectories of sediment particles with different diameters. It can be seen that the diameter of sediment particles directly affects its gravity, buoyancy, and the resistance of water. The larger the diameter of sediment particles, the greater the fluid resistance, the sooner the sediment particles strike the fracture surface, and the more rapidly movement is transformed from translation motion to rolling motion.

From the sediment velocity curves (see Fig. 4), the distribution of particle velocity can be divided into three stages: (1) continuous increase: during this stage, the velocity increases and approaches the peak value, due to the flow of the water phase; (2) rapid decrease: the velocity decreases

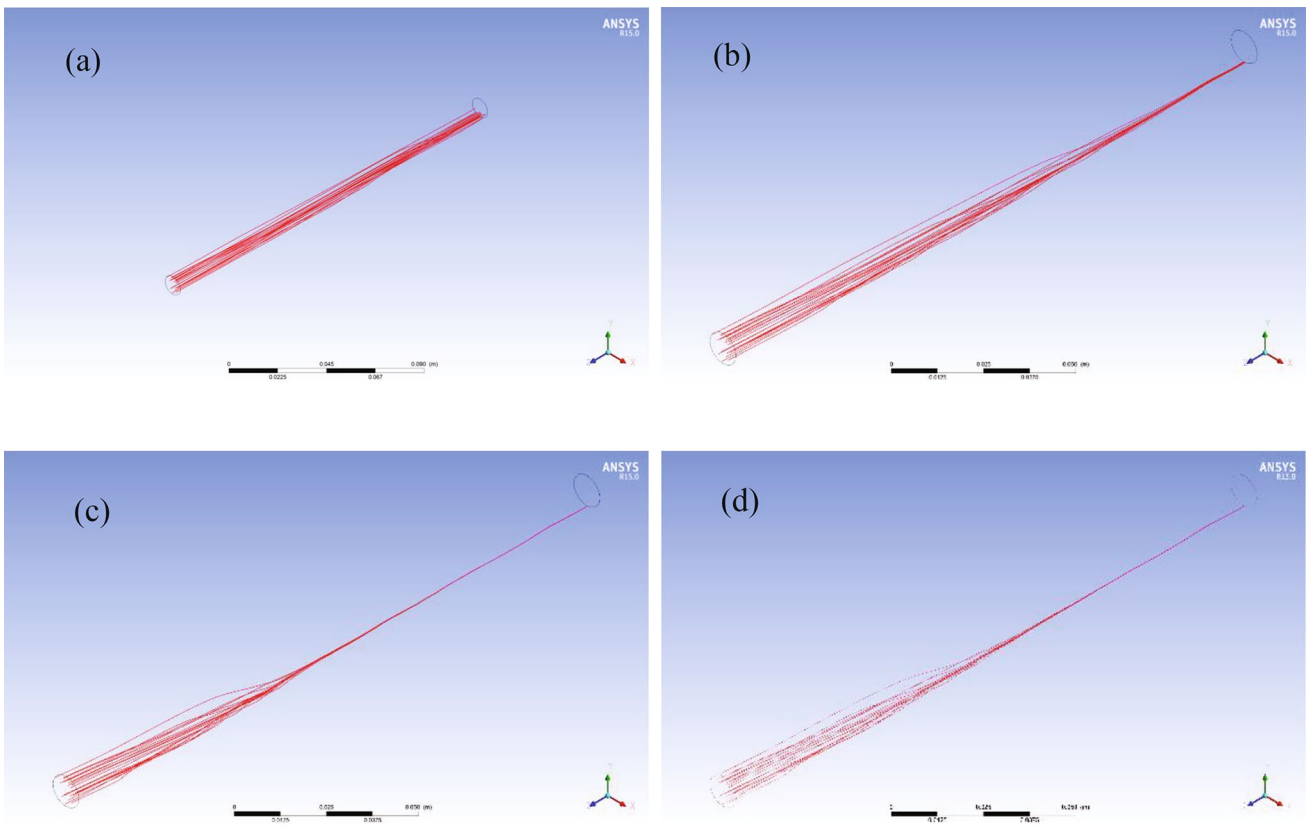

Fig. 3 Particle trajectories of sediment for variable particle diameter. **a** d_s = 0.08 mm; **b** d_s = 0.12 mm; **c** d_s = 0.16 mm; **d** d_s = 0.20 mm

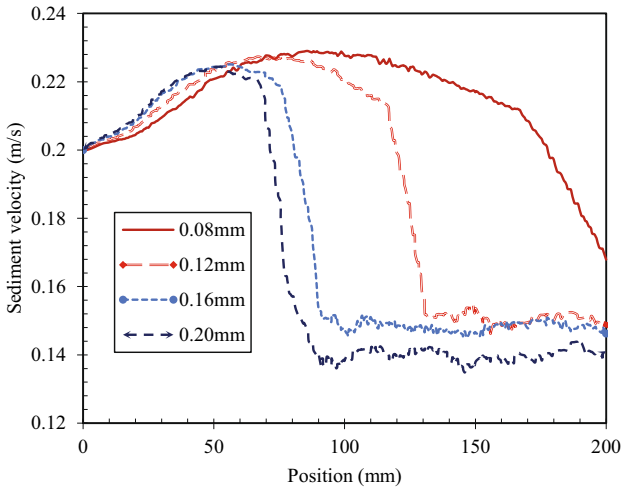

Fig. 4 Distribution of sediment velocity within variable particle diameters

rapidly from the maximum because the gravity, resistance, and thrust of the water reaches equilibrium; the velocity of the water no longer increases, and then the particle velocity begins to decrease due to the significant influence of gravity and thrust. (3) Slow fluctuation: in this stage, the velocity stops decreasing and begins to slightly fluctuate, which is caused by the particles striking and rolling forward to the fracture surface.

In the first stage, the increase in particle velocity is affected by particle size. The larger diameter particles have a greater maximum velocity and reach the maximum velocity in a shorter distance. Based on the above analysis, it appears that the larger the diameter of the particles in the first stage, the greater its buoyancy and water resistance.

Sediment Volume Fraction

When the water–sediment mixture flows through the fractures, the sediment volume fraction is used to reflect the transporting ability of unit mass water carrying the mass of solid particles. As shown in Fig. 5a, as the sediment volume fraction increases, the maximum pressure within the fracture increases exponentially, and the pressure drop of the unit length increases (for fractures with the same length). As shown in Fig. 5b, the higher the sediment volume fraction, the smaller the maximum sediment velocity. The main reasons are that: the high sediment volume fraction leads to more frequent contact and collisions between the particles, resulting in more kinetic energy loss; then the average velocity of the solid particles is smaller. Figure 5c shows the evolution of turbulent dissipation energy in the tube. It indicates that the larger the sediment volume fraction, the greater the disturbance of the acceleration effect of the sediment

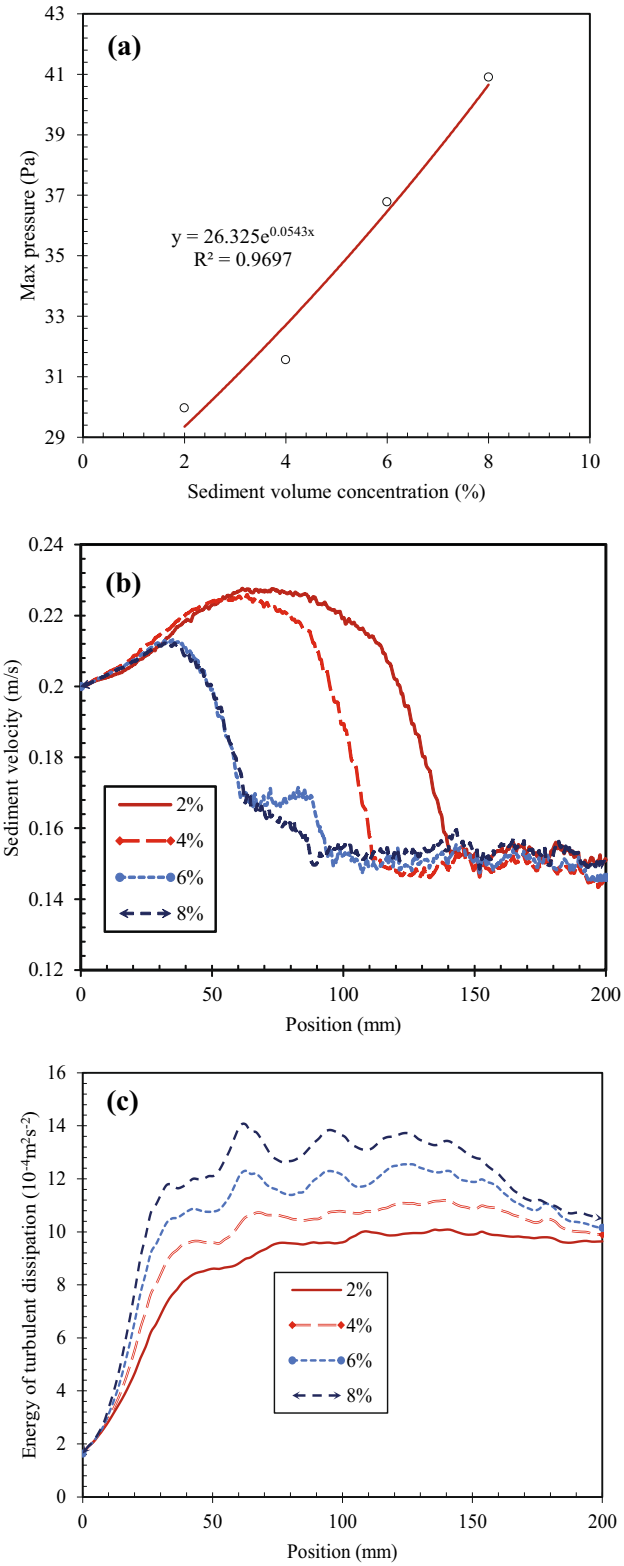

Fig. 5 Characteristics of water–sediment flow within variable sediment volume fraction **a** Max pressure **b** Distribution of sediment velocity **c** Distribution of turbulent dissipation energy

particles to the surrounding liquid in the previous period. Therefore, the turbulent kinetic energy is also greater.

Initial Water Phase Velocity

The simulation results show that with increased initial water phase velocity, the pressure drop in the fracture gradually increases (see supplemental Fig. S-4), while the particle velocity fluctuation is relatively flat (Fig. 6). With increased distance to the inlet, the sediment velocity is slowly increased to a value slightly greater than the water velocity, and then this value slows down to slightly less than the water velocity.

For a low-concentration water–sediment mixture flowing through fractures of the rock mass, the resistance mainly comes from the surface friction generated by the relative slip of the sediment and water phases. As the initial water phase velocity increases, the friction and collision among the particles and between the particles and the fracture surface are more violent, so the relative slip velocity between the two phases of water and sediment decreases. In return, the friction between them is reduced, resulting in greater kinetic energy loss. Finally, some of the particles settle into the bottom of the fracture to form a sliding bed (Fig. 7), which in turn produces more flow resistance. If the water phase velocity is small (Fig. 7a), the energy loss caused by the friction between the sliding bed and the fracture surface is less than the pressure loss. In summary, the pressure loss decreases with decreased water velocity; if the water phase velocity is large (Fig. 7c), then the solid particles are accelerated by the water phase, and most of them do not settle to the bottom of the fracture, but flow out of the fracture with the water

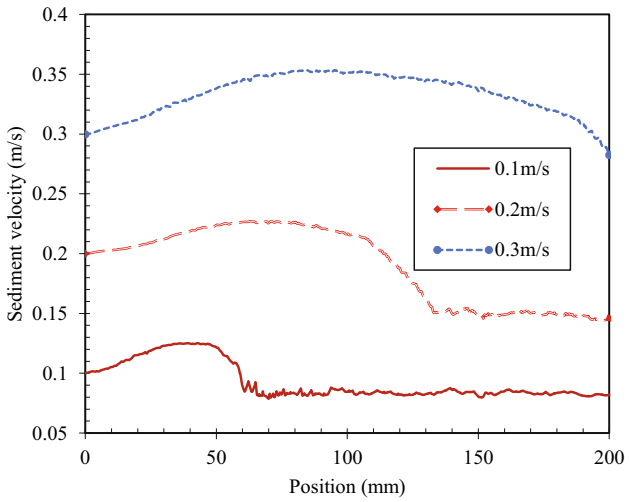

Fig. 6 Distribution of sediment velocity within variable initial water phase velocities

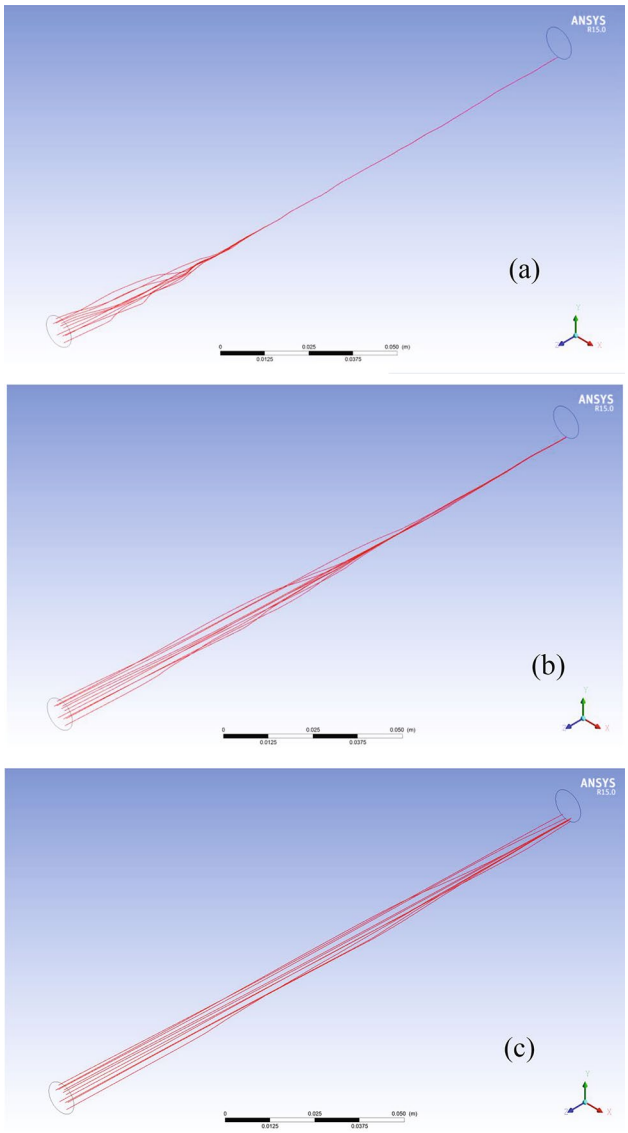

Fig. 7 Particle trajectories of sediment under variable initial water phase velocity. **a** v_0=0.1 m/s; **b** v_0=0.2 m/s; **c** v_0=0.3 m/s

phase. Therefore, particle deposition along the fracture is minimal, and velocity fluctuations are minimal.

Related Experimental Verification

A laboratory-scale test was conducted to validate the numerical model. The test system consisted of a straight glass tube, a water pump with a flow meter, a water–sediment mixer, and a sediment collection device (supplemental Fig. S-5). The straight glass tube was 200 mm in length and 10 mm in inner diameter and placed horizontally. Under the action of the water pump, the water flowed into the mixer, forming a water–sediment mixture. Then, this water–sediment mixture flowed through the glass tube and

eventually flowed into the collection device. To obtain the sediment mass, the mixture was filtered and weighed there.

The sediment volume fraction and water phase velocity were adjusted by the water–sediment mixing device and water pump, respectively. The particle sizes were set as: 0.06–0.10 mm (Group 0.08 mm), 0.10–0.14 mm (Group 0.12 mm), 0.14–0.18 mm (Group 0.1 6 mm), and 0.18–0.22 mm (Group 0.20 mm) (Table 2).

The testing value (TV) of the mean particle velocity $\overline{v}_s$ was calculated by Eq. 14:

$$\overline{v}_s = \frac{M}{\rho_s ST} \tag{14}$$

where M is the mass of sediment particles collected; T is the collection time; and S is the cross-sectional area of the glass tube. For the model solution, the calculated value (CV) of the mean particle velocity $\overline{v}_{sc}$ is obtained by:

$$\overline{v}_{sc} = \frac{\int_0^l v_s(x)dx}{l} \tag{15}$$

The difference between the TV and the CV is described by the absolute percentage error (APE):

$$APE = \left| \frac{\overline{v}_s - \overline{v}_{sc}}{\overline{v}_s} \right| \times 100\% \tag{16}$$

Supplemental Fig. S-6 compares the TV and the CV. It is obvious that the CV and TV curves have the same trend. In addition, the APE of the model increases with increased water phase velocity and decreases in the sediment volume fraction and particle diameter. Meanwhile, the mean values of APEs for variable particle diameter, volume fraction, and water phase velocity is 5.0, 5.1, and 5.2%, respectively, which indicates that the model was highly accurate.

Table 2 Details of verification test

Sample	Sediment particle diameter (mm)	Sediment particle concentration (%)	Initial water phase velocity (m s^{-1})
1–4	0.08, 0.12, 0.16, 0.20	4	0.2
5–8	0.12	2, 4, 6, 8	0.2
9–11	0.12	4	0.1, 0.2, 0.3

Influence of Fracture Characteristics on the Water–Sediment Flow

The influence of fracture characteristics, such as the fracture width, inclination angle, and bending angle, on the water–sediment flow should be considered. However, given the limited experimental conditions, it was not possible to simulate these fracture characteristics. Nevertheless, the numerical model was verified as being highly precise, so the two-phase flow resistance model was used to investigate the effect of fracture characteristics (Table 3).

Fracture Width

Supplemental Fig. S-7 shows the pressure distribution of fractures with variable fracture widths. It can be seen that the water–sediment two-phase flow conditions varies as the fracture width changes. The pressure distribution in the fracture with a width of 5 mm presents a gradient distribution that is basically perpendicular to the fracture direction, while a fracture with a width of 20 mm presents a pressure gradient distribution with a certain inclination angle. Figure 8a shows the variable maximum pressure for different fracture widths. It is obvious that the maximum pressure decreases exponentially with as the fracture width increases.

The distribution of turbulent dissipation energy is depicted in Fig. 8b. The turbulent dissipation energy increases significantly near the inlet ($x < 50$ mm) in a fracture with a width of 5 mm, while in a wider fracture, this growth becomes flatter; there is no obvious growth stage in a 20 mm wide fracture. In addition, at all positions, the turbulent dissipation energy increases gradually with the decrease of the width. This phenomenon indicates that the interaction between sediment particles and the fracture surface is stronger in a narrower fracture, and the loss of particle kinetic energy is more intense there.

Fracture Inclination Angle

Supplemental fig. S-8 and Fig. 9 show simulation results for various inclination angles. As shown in Fig. S-8, the

Table 3 Numerical schemes of fracture characteristics on water–sediment flow for sediment particle diameter 0.12 mm, a sediment particle concentration of 4%, and an initial water phase velocity of 0.2 m s^{-1}

Schemes	Fracture width (mm)	Fracture inclination angle (°)	Fracture bending angle (°)
Scheme 4 Fracture width	5, 10, 15, 20	0	0
Scheme 5 Fracture inclination angle	10	0, 15, 30, 45	0
Scheme 6 Fracture bending angle	10	0	15, 30, 60, 90

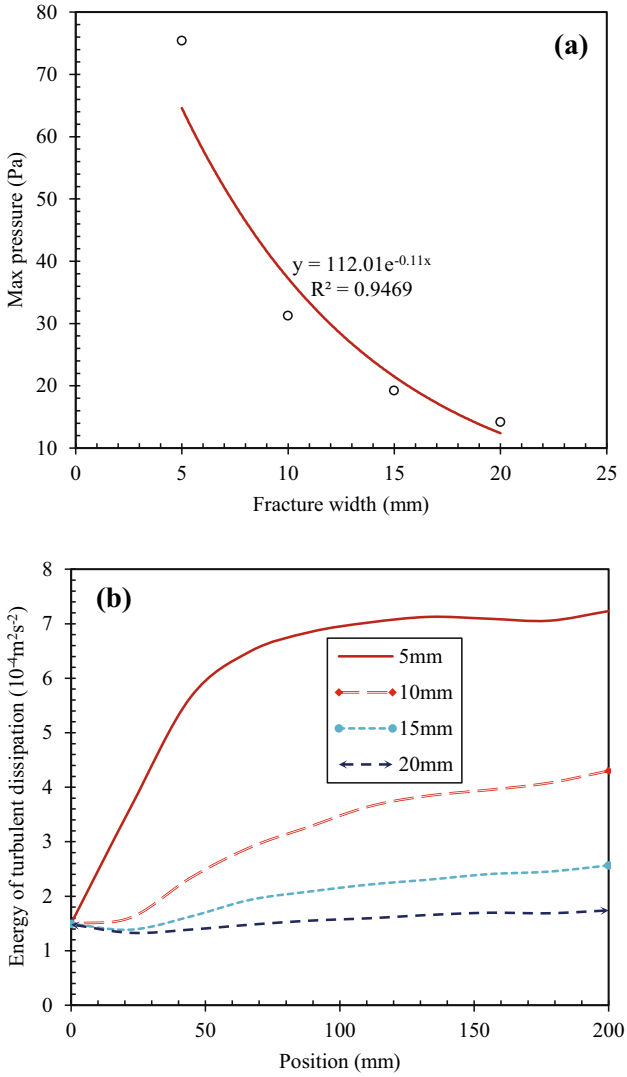

Fig. 8 Characteristics of water–sediment flow in fracture for variable fracture width **a** Max pressure **b** Distribution of turbulent dissipation energy

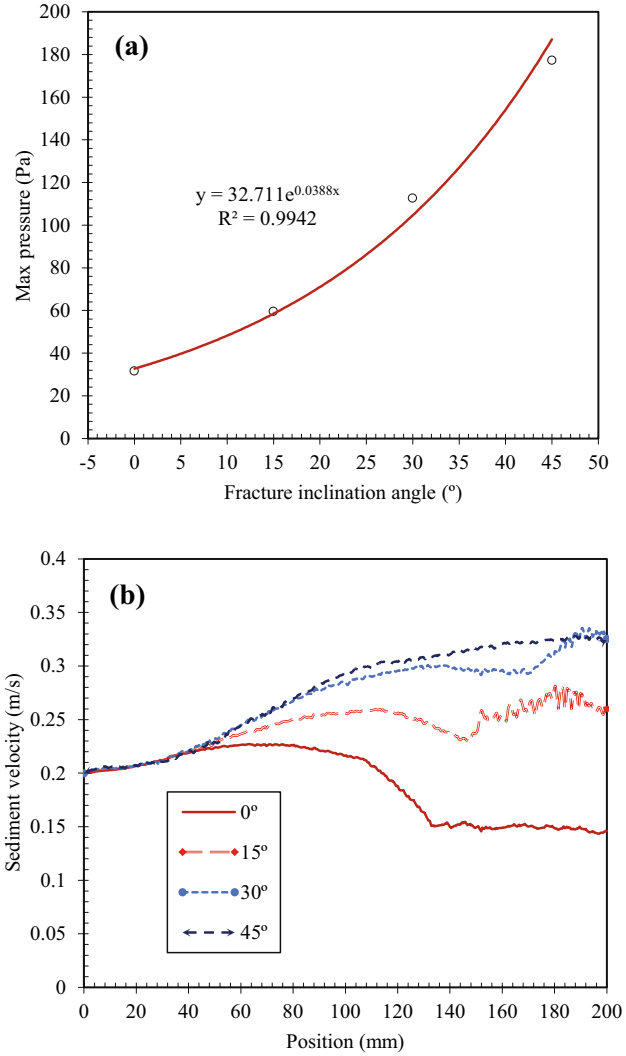

Fig. 9 Characteristics of water–sediment flow within variable fracture inclination angle **a** Max pressure **b** Distribution of sediment velocity

maximum pressure occurs at the inlet of the fracture. As the inclination angle is increased, the maximum pressure increases exponentially (Fig. 9a). In fractures with a larger inclination angle, water and sediment flow to a higher place under the action of water pressure. More energy is required in this process, resulting in greater water pressure at the inlet.

Figure 9b shows the distribution of sediment velocity with varied fracture inclination angles. Near the water inlet, the sediment velocity increases as the distance to the water inlet increases. Then, for most samples ($\varphi < 45°$), the sediment velocity decreases and then fluctuates around a certain value near the outlet, while sediment velocity does not decrease for samples with the highest inclination. The larger the inclination angle, the higher the peak value and the longer sediment velocity increases. It was therefore concluded that smaller fracture inclination angles decrease the resistance, and increase the distance required for sediment particles to change from translation to a rolling motion.

Fracture Bending Angle

The fracture bending angle largely determines the movement of the water–sediment flow, and fracture boundaries are a great obstacle to two-phase fluids. Our investigation of water–sediment two-phase flow in fractures with different bending angles indicates that: (1) as the bending angle increases, pressure accumulation at the entrance of the fracture becomes increasingly obvious. This means that the larger the bending angle, the greater the resistance of the fracture surface to the two-phase fluid, and the easier it is to form a blockage (supplemental Fig. S-9). (2) In

a curved fracture, the flow of sediment particles is more strongly affected by resistance from the fracture boundary than from the middle of the fracture. The velocity of particles near the fracture boundary begins to decrease, while inner particles are less affected (supplemental Fig. S-10). (3) Figure 10 illustrates that the greater the fracture bending angle, the more pronounced the velocity decay of the solid particles. For example, in a fracture with a bending angle of 15°, the velocity of solid particles in the first 100 mm does not change substantially. However, if the bending angles of the fractures are 30°, 60°, and 90°, respectively, a significant decline occurs. Moreover, the greater the bending angle, the more obvious the decline. If the bending angle of the fracture is 60°, the velocity sharply fluctuates, which is mainly due to violent collisions of particles with the fracture surface.

Discussions

Technology to Prevent Water–Sediment Inrush

Since weakening the effect of water and sediment flow can prevent water–sediment inrush, the following measures can be theoretically be taken to prevent such disasters: (1) reduce the fracture width; (2) increase the tilt angle and the fracture bending; (3) increase the sediment particle diameter; (4) reduce the volume fraction; and (5) decrease the flow rate. In practice, the following measures can be taken to prevent water–sediment disasters:

1. Backfilling of surface fractures: surface fractures caused by mining should be quickly backfilled to shut off water and sediment inrush channels.

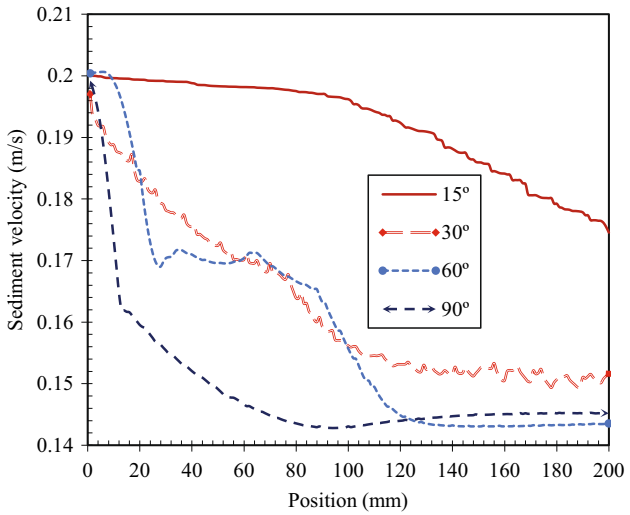

Fig. 10 Distribution of sediment velocity at different bending angles

2. Grouting and reinforcement: in addition, the reinforcement of rock layers above a water-conducting fracture can prevent the mixture of water and sediment from entering the fracture channels.
3. Dewatering and depressurization: reducing the aquifer water level will reduce the probability of aeolian sediment being liquefied; reducing the water pressure will reduce the water's power and velocity; and increasing the sediment volume fraction will promote the flow resistance of the water–sediment fluid.

Water–Sediment Inrush Mitigation Technology

Traditional abatement efforts involve draining the water and sediment after a disaster, which can cause the water and sediment to continue to flow from the surface into the mines. Instead, the focus should be changed to quickly blocking the water–sediment inrush fracture channel), reducing fracture channels in the rock mass, minimizing the ability of water and sediment to flow, and carrying out grouting reinforcement. In other words, countermeasures should be align with reducing pipe flow to fracture flow, reducing fracture flow to pore flow, grouting and sealing conductive channels, and weakening the fluid's sediment-carrying capacity.

Conclusions

Based on the theory of two-phase flow, we established a water–sediment two-phase flow resistance model. First, governing equations of water and sediment phases were built, and then, the effect of equivalent resistance and the interactive force of the water–sediment were considered. Based on the solution conditions, the pressure and velocity distribution of the water–sediment mixed flow in fractures were analysed. The main conclusions are:

1. Based on the proposed model, the influence of fluid characteristics (sediment particle diameter, sediment volume fraction, initial water phase velocity) on flow resistance were defined. We concluded that an increased sediment diameter results in the rise of resistance and less distance required to convert particle flow into a rolling motion. The evolution of sediment velocity can be divided into three stages, i.e., continuous increase, rapid decrease, and slow fluctuations.
2. With an increased sediment volume fraction, the maximum pressure increases exponentially, the mean velocity of the sediment particles decreases, and the turbulent kinetic energy increases. With an increase of the initial velocity of the water phase, the unit pressure drop loss in the fracture increases gradually, and particle velocity fluctuations becomes gentle. Relatively few particles are

deposited in the fracture channel; instead, most of the sediment particles flow out with the fluid.

3. This model was verified by a laboratory-scale test, which showed that the absolute percentage error (APE) of the model increases as the flow velocity increases and the sediment volume fraction and average particle diameter decrease. In addition, the low APEs revealed in all samples suggest that the numerical model is highly precise.
4. Based on the verified model, the influence of the fracture characteristics (fracture width, inclination angle, bending angle) on the flow resistance was analyzed. The results showed that these fracture characteristics have a great influence on water–sediment two-phase flow. With a decreased fracture width, or an increase in either the inclination angle or the bending angle, the fracture's resistance to the two-phase flow increases. The velocity attenuation of sediment particles is obvious, which is mainly caused by the collision of particles with the fracture surface.
5. Preliminary prevention techniques for water–sediment inrush (surface fracture backfilling, grouting reinforcement, dewatering, and depressurization) were proposed. The main idea of these countermeasures is to reduce pipe flow to fracture flow, reduce fracture flow to pore flow, grout and seal the conductive channel, and weaken the fluid's sediment carrying capacity.

Acknowledgements This work was supported by the National Natural Science Foundation of China (41977238 and 51804339), the Young Elite Scientists Sponsorship by CAST (YESS20190175), the Special Fund for the Construction of Innovative Provinces in Hunan (2019RS2007), the China Postdoctoral Science Foundation (2019T120715 and 2018M640760), the Open Project Fund for State Key Laboratory of Mining Disaster Prevention and Control Co-founded by Shandong Province (MDPC201901) and the Fundamental Research Fund for the Central Universities of CSU (2019zzts675).

References

Berkowitz B (2002) Characterizing flow and transport in fractured geological media: a review. Adv Water Resour 25:861–884. https://doi.org/10.1016/s0309-1708(02)00042-8

Brouwers LB, Dippenaar MA (2019) Partially saturated flow from sand into a discrete smooth open vertical fracture at the soil–rock interface: experimental studies. Bull Eng Geol Environ 78:2575–2590. https://doi.org/10.1007/s10064-018-1258-x

Elbaz K, Shen JS, Arulrajah A, Horpibulsuk S (2016) Geohazards induced by anthropic activities of geoconstruction: a review of recent failure cases. Arab J Geosci 9:708. https://doi.org/10.1007/s12517-016-2740-z

Fan H, Zheng H (2013) MRT-LBM-based numerical simulation of seepage flow through fractal fracture networks. Sci China Technol Sci 56:3115–3122. https://doi.org/10.1007/s11431-013-5402-3

Fan G, Zhang D, Zhang S, Zhang C (2018) Assessment and prevention of water and sand inrush associated with coal mining under a water-filled buried gully: a case study. Mine Water Environ 37:565–576. https://doi.org/10.1007/s10230-017-0487-8

Gu H, Tao M, Li X, Momeni A, Cao W (2019) The effects of water content and external incident energy on coal dynamic behaviour. Int J Rock Mech Min Sci 123:104088. https://doi.org/10.1016/j.ijrmms.2019.104088

Guihéneuf N, Boisson A, Bour O, Dewandel B, Perrin J, Dausse A, Viossanges M, Chandra S, Ahmed S, Maréchal JC (2014) Groundwater flows in weathered crystalline rocks: impact of piezometric variations and depth-dependent fracture connectivity. J Hydrol 511:320–334. https://doi.org/10.1016/j.jhydrol.2014.01.061

Hamm S-Y, Kim M, Cheong J-Y, Kim J-Y, Son M, Kim T-W (2007) Relationship between hydraulic conductivity and fracture properties estimated from packer tests and borehole data in a fractured granite. Eng Geol 92:73–87. https://doi.org/10.1016/j.enggeo.2007.03.010

Huang Y-H, Yang S-Q (2019) Mechanical and cracking behavior of granite containing two coplanar flaws under conventional triaxial compression. Int J Damage Mech 28:590–610. https://doi.org/10.1177/1056789518780214

Huang Z, Jiang Z, Zhu S, Wu X, Yang L, Guan Y (2016) Influence of structure and water pressure on the hydraulic conductivity of the rock mass around underground excavations. Eng Geol 202:74–84. https://doi.org/10.1016/j.enggeo.2016.01.003

Huang Z, Li X, Li S, Zhao K, Zhang R (2018) Investigation of the hydraulic properties of deep fractured rocks around underground excavations using high-pressure injection tests. Eng Geol 245:180–191. https://doi.org/10.1016/j.enggeo.2018.07.020

Huang Y-H, Yang S-Q, Tian W-L (2019a) Crack coalescence behavior of sandstone specimen containing two pre-existing flaws under different confining pressures. Theor Appl Fracture Mech 99:118–130. https://doi.org/10.1016/j.tafmec.2018.11.013

Huang Y, Li J, Ma D, Gao H, Guo Y, Ouyang S (2019b) Triaxial compression behaviour of gangue solid wastes under effects of particle size and confining pressure. Sci Total Environ 693:133607. https://doi.org/10.1016/j.scitotenv.2019.133607

Javadi M, Sharifzadeh M, Shahriar K (2010) A new geometrical model for non-linear fluid flow through rough fractures. J Hydrol 389:18–30. https://doi.org/10.1016/j.jhydrol.2010.05.010

Ju F, Xiao M, He Z, Ning P, Huang P (2018) Study on fracture and stress evolution characteristics of ultra-thick hard sandstone roof in the fully mechanized mining face with large mining height: a case study of Xiaojihan coal mine in western China. Adv Civil Eng 2018:12. https://doi.org/10.1155/2018/5474165

Kristinof R, Ranjith PG, Choi SK (2010) Finite element simulation of fluid flow in fractured rock media. Environ Earth Sci 60:765–773. https://doi.org/10.1007/s12665-009-0214-2

Li LC, Tang CA, Li G, Wang SY, Liang ZZ, Zhang YB (2012) Numerical simulation of 3D hydraulic fracturing based on an improved flow-stress-damage model and a parallel FEM technique. Rock Mech Rock Eng 45:801–818. https://doi.org/10.1007/s00603-012-0252-z

Li S, Wang J, Li L, Shi S, Zhou Z (2019) The theoretical and numerical analysis of water inrush through filling structures. Math Comput Simulat 162:115–134. https://doi.org/10.1016/j.matcom.2018.12.014

Liang YK, Sui WH, Qi JF (2019) Experimental investigation on chemical grouting of inclined fracture to control sand and water flow. Tunn Undergr Space Technol 83:82–90. https://doi.org/10.1016/j.tust.2018.09.038

Liu Y, Li S (2016) Influence of particle size on non-Darcy seepage of water and sediment in fractured rock. SpringerPlus 5:2099. https://doi.org/10.1186/s40064-016-3778-9

Liu J, Chen W, Yuan J, Li C, Zhang Q, Li X (2017) Groundwater control and curtain grouting for tunnel construction in completely

weathered granite. Bull Eng Geol Environ 77:515–531. https://doi.org/10.1007/s10064-017-1003-x

Liu J, Chen W, Liu T, Yu J, Dong J, Nie W (2018) Effects of initial porosity and water pressure on seepage-erosion properties of water inrush in completely weathered granite. Geofluids 2018:1–11. https://doi.org/10.1155/2018/4103645

Liu W, Yao J, Chen Z, Zhu W (2019) An exact analytical solution of moving boundary problem of radial fluid flow in an infinite low-permeability reservoir with threshold pressure gradient. J Petrol Sci Eng 175:9–21. https://doi.org/10.1016/j.petrol.2018.12.025

Liu H, Zhu W, Yu Y, Xu T, Li R, Liu X (2020) Effect of water imbibition on uniaxial compression strength of sandstone. Int J Rock Mech Min Sci 127:104200. https://doi.org/10.1016/j.ijrmms.2019.104200

Ma D, Rezania M, Yu H-S, Bai H-B (2017) Variations of hydraulic properties of granular sandstones during water inrush: effect of small particle migration. Eng Geol 217:61–70. https://doi.org/10.1016/j.enggeo.2016.12.006

Ma D, Duan H, Li X, Li Z, Zhou Z, Li T (2019a) Effects of seepage-induced erosion on nonlinear hydraulic properties of broken red sandstones. Tunn Undergr Space Technol 91:102993. https://doi.org/10.1016/j.tust.2019.102993

Ma D, Duan HY, Liu JF, Li XB, Zhou ZL (2019b) The role of gangue on the mitigation of mining-induced hazards and environmental pollution: an experimental investigation. Sci Total Environ 664:436–448. https://doi.org/10.1016/j.scitotenv.2019.02.059

Ma D, Wang J, Cai X, Ma X, Zhang J, Zhou Z, Tao M (2019c) Effects of height/diameter ratio on failure and damage properties of granite under coupled bending and splitting deformation. Eng Fract Mech 220:106640. https://doi.org/10.1016/j.engfracmech.2019.106640

Ma D, Wang J, Li Z (2019d) Effect of particle erosion on mining-induced water inrush hazard of karst collapse pillar. Environ Sci Poll Res 26:19719–19728. https://doi.org/10.1007/s11356-019-05311-x

Peker SM, Helvaci SS (2008) Solid-liquid two phase flow. Elsevier, Amsterdam

Peng K, Zhou J, Zou Q, Zhang J, Wu F (2019) Effects of stress lower limit during cyclic loading and unloading on deformation characteristics of sandstones. Constr Build Mater 217:202–215. https://doi.org/10.1016/j.conbuildmat.2019.04.183

Poesen J, Nachtergaele J, Verstraeten G, Valentin C (2003) Gully erosion and environmental change: importance and research needs. CATENA 50:91–133. https://doi.org/10.1016/S0341-8162(02)00143-1

Qian X, Xia C, Gui Y, Zhuang X, Yu Q (2019) Study on flow regimes and seepage models through open rough-walled rock joints under high hydraulic gradient. Hydrogeol J 27:1329–1343. https://doi.org/10.1007/s10040-018-01914-9

Ren F, Ma G, Wang Y, Li T, Zhu H (2017) Unified pipe network method for simulation of water flow in fractured porous rock. J Hydrol 547:80–96. https://doi.org/10.1016/j.jhydrol.2017.01.044

Sahimi M (2011) Flow and transport in porous media and fractured rock: from classical methods to modern approaches. Wiley, New York

Sun WJ, Wu Q, Dong DL, Jiao J (2012) Avoiding coal-water conflicts during the development of China's large coal-producing regions. Mine Water Environ 31:74–78. https://doi.org/10.1007/s10230-012-0173-9

Tao M, Ma A, Cao W, Li X, Gong F (2017) Dynamic response of pre-stressed rock with a circular cavity subject to transient loading. Int J Rock Mech Min Sci 99:1–8. https://doi.org/10.1016/j.ijrmms.2017.09.003

Valentin C, Poesen J, Li Y (2005) Gully erosion: impacts, factors and control. CATENA 63:132–153. https://doi.org/10.1016/j.catena.2005.06.001

Wang L, Kong H (2018) Variation characteristics of mass-loss rate in dynamic seepage system of the broken rocks. Geofluids 2018:1–17. https://doi.org/10.1155/2018/7137601

Wang Y, Geng F, Yang S, Jing H, Meng B (2019) Numerical simulation of particle migration from crushed sandstones during groundwater inrush. J Hazard Mater 362:327–335. https://doi.org/10.1016/j.jhazmat.2018.09.011

Xu P, Yu B, Qiao X, Qiu S, Jiang Z (2013) Radial permeability of fractured porous media by Monte Carlo simulations. Int J Heat Mass Transf 57:369–374. https://doi.org/10.1016/j.ijheatmasstransfer.2012.10.040

Yang W, Jin L, Zhang X (2019) Simulation test on mixed water and sand inrush disaster induced by mining under the thin bedrock. J Loss Prevent Proc 57:1–6. https://doi.org/10.1016/j.jlp.2018.11.007

Zhang HQ, He YN, Tang CA, Ahmad B, Han LJ (2008) Application of an improved flow-stress-damage model to the criticality assessment of water inrush in a mine: a case study. Rock Mech Rock Eng 42:911. https://doi.org/10.1007/s00603-008-0004-2

Zhang R, Jiang Z, Zhou H, Yang C, Xiao S (2014) Groundwater outbursts from faults above a confined aquifer in the coal mining. Nat Hazard 71:1861–1872. https://doi.org/10.1007/s11069-013-0981-7

Zhang G, Zhang K, Wang L, Wu Y (2015a) Mechanism of water inrush and quicksand movement induced by a borehole and measures for prevention and remediation. Bull Eng Geol Environ 74:1395–1405. https://doi.org/10.1007/s10064-014-0714-5

Zhang ZZ, Bai JB, Chen Y, Yan S (2015b) An innovative approach for gob-side entry retaining in highly gassy fully-mechanized longwall top-coal caving. Int J Rock Mech Min Sci 80:1–11. https://doi.org/10.1016/j.ijrmmis.2015.09.001

Zhou Q, Herrera J, Hidalgo A (2018) The numerical analysis of fault-induced mine water inrush using the extended finite element method and fracture mechanics. Mine Water Environ 37:185–195. https://doi.org/10.1007/s10230-017-0461-5